

Creative Commons Attribution 4.0 International (CC BY 4.0)

<https://creativecommons.org/licenses/by/4.0/>

Access to this work was provided by the University of Maryland, Baltimore County (UMBC) ScholarWorks@UMBC digital repository on the Maryland Shared Open Access (MD-SOAR) platform.

Please provide feedback

Please support the ScholarWorks@UMBC repository by emailing scholarworks-group@umbc.edu and telling us what having access to this work means to you and why it's important to you. Thank you.



A continuous 2011-2022 record of fine particulate matter (PM_{2.5}) in East Asia at daily 2-km resolution from geostationary satellite observations: population exposure and long-term trends

Drew C. Pendergrass¹, Daniel J. Jacob¹, Yujin J. Oak¹, Jeewoo Lee², Minseok Kim², Jhoon Kim², Seoyoung Lee^{3,4}, Shixian Zhai⁵, Hitoshi Irie⁶, and Hong Liao⁷.

¹School of Engineering and Applied Sciences, Harvard University, Cambridge, Mass., USA

²Department of Atmospheric Sciences, Yonsei University, Seoul, South Korea

³Goddard Earth Sciences Technology and Research (GESTAR) II, University of Maryland Baltimore County, Baltimore, MD, USA

10 ⁴NASA Goddard Space Flight Center, Greenbelt, Md., USA

⁵Earth and Environmental Sciences Programme and Graduation Division of Earth and Atmospheric Sciences, Faculty of Science, The Chinese University of Hong Kong, Sha Tin, Hong Kong SAR, China

⁶Center for Environmental Remote Sensing (CEReS), Chiba University, Chiba, Japan

15 ⁷Jiangsu Key Laboratory of Atmospheric Environment Monitoring and Pollution Control, Jiangsu Collaborative Innovation Center of Atmospheric Environment and Equipment Technology, School of Environmental Science and Engineering, Nanjing University of Information Science and Technology, Nanjing, Jiangsu, China

Correspondence to: Drew Pendergrass (pendergrass@g.harvard.edu)

Abstract. We construct a continuous 24-h daily fine particulate matter (PM_{2.5}) record with 2×2 km² resolution over eastern China, South Korea, and Japan for 2011-2022 by applying a random forest (RF) algorithm to aerosol optical depth (AOD) observations from the Geostationary Ocean Color Imager (GOCI) I and II satellite instruments. The RF uses PM_{2.5} observations from the national surface networks as training data. PM_{2.5} network data starting in 2015 in South Korea are extended to pre-2015 with a RF trained on other air quality data available from the network including PM₁₀. PM_{2.5} network data starting in 2014 in China are supplemented by pre-2014 data from the US embassy and consulates. Missing AODs in the GOCI data are gap-filled by a separate RF fit. We show that the resulting GOCI PM_{2.5} dataset is successful in reproducing the surface network observations including extreme events, and that the network data in the different countries are representative of population-weighted exposure. We find that PM_{2.5} peaked in 2014 (China) and 2013 (South Korea, Japan), and has been decreasing steadily since with no region left behind. We quantify the population in each country exposed to annual PM_{2.5} in excess of national ambient air quality standards and how this exposure evolves with time. The long record for the Seoul Metropolitan Area (SMA) shows a steady decrease from 2013 to 2022 that was not present in the first five years of AirKorea network PM_{2.5} measurements. Mapping of an extreme pollution event in Seoul with GOCI PM_{2.5} shows a predicted distribution indistinguishable from the dense urban network observations, while our previous 6×6 km² product smoothed local features. Our product should be useful for public health studies where long-term spatial continuity of PM_{2.5} information is essential.



1. Introduction

Outdoor fine particulate matter (PM_{2.5}, less than 2.5 µm in diameter) is a leading cause of morbidity and mortality, with exposure leading to 8.9 million deaths worldwide in 2015 and increased diagnoses of
 40 respiratory, cardiovascular, and neurodegenerative diseases (Dominici et. al., 2006; Kioumourtzoglou et. al., 2016; Burnett et. al., 2018 Wei et. al., 2019). East Asian countries experience particularly high concentrations of PM_{2.5}. China introduced its Action Plan on Prevention and Control of Air Pollution in 2013 (Chinese State Council, 2013) and South Korea introduced its Comprehensive Action Plan on Fine Dust in 2017 (Joo, 2018). As a result, concentrations declined in the latter half of the 2010s
 45 (Pendergrass et al., 2022). However, the publicly available archive of PM_{2.5} measurements from national surface networks only started in 2014 in China and in 2015 in South Korea, and even today they are relatively sparse for public health applications. Here we use geostationary satellite observations of aerosol optical depth (AOD) from the Geostationary Ocean Color Imager (GOCI) I and II instruments, trained with surface PM_{2.5} data using a machine learning algorithm, to provide complete
 50 2011-2022 daily 24-h coverage of surface PM_{2.5} concentrations at 2×2 km² resolution for eastern China, South Korea, and Japan.

Satellite retrievals of AOD from backscattered solar radiation have long been used to expand surface PM_{2.5} coverage beyond that provided by network sites. Early applications used AOD/PM_{2.5} ratios computed with a chemical transport model (CTM) to infer surface PM_{2.5} from observed AOD
 55 (Liu et al., 2004; van Donkelaar et al., 2006; van Donkelaar et al., 2021) but this may be affected by CTM biases. More recent applications have used machine learning algorithms to train satellite AODs on PM_{2.5} network measurements (Guo et al., 2021; Pendergrass et al., 2022; Wongnakae et al., 2023). Commonly used machine learning algorithms include XGBoost and Random Forest (RF), both based on decision trees, and neural networks; precision tends to be similar across algorithms (Di et al., 2019; Kulkarni et al., 2022). RF approaches are widely used due to their explainability and consistently strong
 60 performance with minimal hyperparameter tuning (Breiman, 2001).

In East Asia, studies inferring PM_{2.5} from satellite AOD data have benefited from new geostationary instruments including GOCI (launched 2010), the Advanced Himawari Imager (AHI, launched 2014), the Advanced Meteorological Imager (AMI, launched 2018), GOCI-II and GEMS
 65 (launched in 2020), which provide continuous hourly or subhourly measurements during daytime (Choi et al., 2018; Lim et al., 2018; Lee et al., 2023; Kim et al., 2023; Cho et al., 2023a). The RF method has been used to infer hourly PM_{2.5} from geostationary AOD (Liu et al., 2022; Tan et al., 2023; Cho et al., 2023b), but geostationary AOD also improves inference of 24-h mean PM_{2.5}; Park et al. (2019) found that an RF algorithm trained to predict PM_{2.5} from GOCI AOD outperformed an otherwise identical one
 70 trained on the MODIS low-earth orbit instrument. Our previous work (Pendergrass et al., 2022) used GOCI I observations to produce a continuous 24-h 6×6 km² PM_{2.5} product for eastern China, South Korea and Japan for the network observation periods (starting in 2014 in China and 2015 in South Korea) and extending to 2019.

Here we use a continuous, gap-filled record of AOD retrieved from GOCI I and its successor
 75 GOCI II on a consistent 2×2 km² grid to infer surface PM_{2.5} at 24-h temporal resolution from March 2011 through the end of 2022 for eastern China, Japan, and South Korea. We make use of an improved AOD gap-filling procedure by using a separate RF fit trained to reproduce AOD data. To provide



continuity in training across the study domain from 2011 to present, we additionally develop and evaluate a virtual network $PM_{2.5}$ record prior to 2015 in South Korea by training an RF on network observations of coarse particulate matter (PM_{10}) and other air pollutants. In China, we make use of US embassy and consulate $PM_{2.5}$ data to train the RF before 2014. We use the resulting GOCI $PM_{2.5}$ dataset to analyze urban and regional trends in $PM_{2.5}$ including population exposures.

2. Methods

Pendergrass et al. (2022) used GOCI I AOD observations to produce a continuous 24-h $6 \times 6 \text{ km}^2$ $PM_{2.5}$ product for eastern China, South Korea and Japan for the surface network observation periods (starting in 2014 in China, 2015 in South Korea, and 2011 in Japan) and extending to the end of 2019. It gap-filled missing GOCI I AOD data by blending a CTM simulation with statistical interpolation (inverse distance weighted means).

Here we improve on Pendergrass et al. (2022) in several major ways. First, we extend the AOD record using the GOCI II instrument to cover the 2011-2022 period, and replace the $6 \times 6 \text{ km}^2$ GOCI I AOD with a $2 \times 2 \text{ km}^2$ GOCI I AOD retrieval (section 2.1). We replace the statistical AOD gap-filling method of Pendergrass et al. (2022) with an additional AOD RF fit (section 2.2). To avoid biased $PM_{2.5}$ estimates in South Korea prior to the beginning of the AirKorea national network observations in 2015, we use an additional RF to infer surface observations of $PM_{2.5}$ in South Korea at the network sites using measurements of other air quality variables including PM_{10} starting from 2011 (section 2.3). In China, we avoid extrapolation bias by supplementing surface network data with data from the US embassy and consulates, which date from 2011. Finally, we train an RF on the gap-filled AOD and other predictor variables to construct a continuous 24-h $2 \times 2 \text{ km}^2$ $PM_{2.5}$ product for China, South Korea, and Japan covering the 2011-2022 period (section 2.4). Table 1 lists the predictor variables for all of the RFs used in this work.

We evaluate how each RF performs and learns via a 10-fold crossvalidation procedure and Shapley analysis. The crossvalidation measures how well an RF can make predictions based on more limited training data. For each fold of the crossvalidation, we leave out a randomly selected 10% of sites entirely from training; in this way, the crossvalidation measures the ability of the RF to generalize spatially to unseen sites. We compare RF-predicted AOD and $PM_{2.5}$ (24-h and annual) to the withheld observed AOD and $PM_{2.5}$ using four metrics: the root mean square error (RMSE); the RMSE divided by mean observed value (relative RMSE, or RRMSE); the coefficient of determination (R^2); and the mean bias computed by averaging the difference between predicted and observed values (MB). To determine the contributions of training variables to the overall RF estimate, we use the SHapley Additive exPlanations (SHAP) analysis as implemented by the TreeExplainer algorithm (Lundberg et al., 2020). This method allocates a SHAP value, in the same unit as the target variable ($\mu\text{g m}^{-3}$ for $PM_{2.5}$, unitless for AOD), to each predictor variable and can be interpreted as the importance of that variable to the trained RF algorithm. All RFs are produced using the Python module scikit-learn (Pedregosa et al., 2011).

Table 1. Random Forest predictor variables^a



GOCI (gap-filled) and GEOS-Chem

GOCI I AOD 8-h average (0:30-7:30 UTC) at 550 nm wavelength (2011-2020)

GOCI II AOD 10-h average (23:15-8:15 UTC) at 550 nm wavelength (2021-2022)

Gaspari-Cohn missingness factor α^b

Bias-corrected GEOS-Chem monthly mean AOD^c

Meteorology^d

Boundary layer height (m)[†]

10-m meridional wind (m s^{-1})*

10-m zonal wind (m s^{-1})*

2-m temperature (K)*

2-m relative humidity^e (%)*

Sea-level pressure (Pa)[†]

KORUSv5 emissions^f

NO_x ($\text{molec m}^{-2} \text{s}^{-1}$)

SO_2 ($\text{molec m}^{-2} \text{s}^{-1}$)

NH_3 ($\text{molec m}^{-2} \text{s}^{-1}$)

Land use

Land cover type (cropland, urban, rural)^g

Population density^h

Elevationⁱ

Normalized Difference Vegetation Index (NDVI)^j

Metadata

Country categorical variables^k

Day of year

Year

AirKorea surface air quality data^l

CO (ppm)

NO_2 (ppm)

O_3 (ppm)

SO_2 (ppm)

PM_{10} ($\mu\text{g m}^{-3}$)

Yellow dust categorical variable (T/F)

^aThese predictor variables are used for three separate RF fits: (1) GOCI $\text{PM}_{2.5}$, (2) imputing pre-2015 $\text{PM}_{2.5}$ at AirKorea sites from PM_{10} and other predictors, and (3) gap-filling GOCI AOD. Unless otherwise noted, the data are used in all three RFs and are mapped onto the $2 \times 2 \text{ km}^2$ GOCI grid cells.

^bWeighting factor with a value of 1 if AOD is retrieved successfully at least once in a given day in a given $2 \times 2 \text{ km}^2$ grid cell and descending to 0 as distance to the nearest successful retrieval increases. Not used to in the GOCI AOD gap-filling RF. See section 2.2.

^cSimulation from Zhai et al. (2021) at $0.5^\circ \times 0.625^\circ$ resolution and corrected to annual mean GOCI observations on the $2 \times 2 \text{ km}^2$ grid.

^dMeteorological data from either the ECMWF hourly $9 \times 9 \text{ km}^2$ resolution ERA5-Land replay of the ERA5 global reanalysis (denoted *) or hourly $30 \times 30 \text{ km}^2$ from ERA5 ([†]), interpolated bilinearly to the GOCI grid and averaged over 24 hours. For coastal pixels missing from the ERA5-Land data, we impute values from ERA5.

^eInferred from temperature and dewpoint using the August-Roche-Magnus approximation (Alduchov and Eskridge, 1996).

^f2015 emissions for East Asia on a $0.1^\circ \times 0.1^\circ$ grid (Woo et al., 2020).



^g Land cover data at 300 m resolution for 2015 is obtained from the from the PROBA-Vegetation (PROBA-V) and Sentinel-3 OLCI (S3 OLCI) time series (<https://cds.climate.copernicus.eu/cdsapp#!/dataset/satellite-land-cover?tab=overview>; CDS, 2019). We aggregate the data to one of three categories based on the most prevalent land cover type within a 2×2 km² GOCI grid cell: urban areas, cropland (irrigated, rainfed, and mosaic but majority cropland), and rural (all other non-water pixels with minimal human modification).

^h 2015 population density at 30 arc second resolution from the Gridded Population of the World v4.11 dataset (CIESIN, 2018)

ⁱ Elevation from the global multi-resolution terrain elevation data 2010 digital elevation model (GMTED2010), corrected and aggregated to 0.0625° resolution by the Tropospheric Emission Monitoring Internet Service (<https://www.temis.nl/data/gmted2010/index.php>; Danielson and Gesch, 2011).

^j Daily Normalized Difference Vegetation Index (NDVI) derived from the NOAA Climate Data Record (CDR) of Advanced Very High Resolution Radiometer (AVHRR) Surface Reflectance and reported at $0.05^\circ \times 0.05^\circ$ resolution (Vermote 2019). A small number of NDVI pixels are missing, which are imputed by first looking for a successful retrieval within two weeks of the day in question and if that fails by inverse distance weighting.

^k Three variables that, for each of eastern China, South Korea, and Japan, have value 1 if a grid cell is within those national borders and 0 otherwise.

^l Used as input in the pre-2015 AirKorea PM_{2.5} RF. Yellow dust variable is true if a dust event (due to transport from China/Mongolia) is observed at a given site that day.

2.1 GOCI, GEOS-Chem, and PM_{2.5} input datasets

GOCI I and II AOD. GOCI I was launched in 2010 by the Korea Aerospace Research Institute (KARI) and recorded data every hour eight times daily at 0.5×0.5 km² pixel resolution over eastern China, the Korean peninsula, and Japan (Choi et al., 2018) until it was shut down in early 2021. GOCI II, launched in February 2020, continues the GOCI mission with improved 0.25×0.25 km² pixel resolution, four additional spectral bands, and ten times daily retrievals over an expanded daytime window (Lee et al., 2023). The Yonsei aerosol retrieval (YAER) algorithm family computes AOD from GOCI measurements by aggregating the native GOCI pixels to improve accuracy and cloud clearing into a 6×6 km² AOD product for GOCI I (GOCI YAER v2; Choi et al., 2018) and a 2.5×2.5 km² AOD product for GOCI-II (GOCI-II YAER; Lee et al., 2023). Lee et al. (2017) showed that fewer GOCI I pixels could be aggregated to produce a higher resolution AOD product with a modest tradeoff in precision. In this work, we use their 2×2 km² GOCI I AOD product (produced from 4×4 GOCI I pixels) which exhibits an R^2 of 0.825 relative to AERONET for 2016 as compared to 0.858 for the standard GOCI YAER v2 6×6 km² AOD product (Lee et al., 2017).

To produce a continuous GOCI AOD training dataset, we first aggregate GOCI I AOD into an 8-h average (0:30-7:30 UTC) and GOCI II AOD into a 10-h average (23:15-8:15 UTC), representing the full daily records of each instrument, then regrid the 2.5×2.5 km² GOCI II AOD to the 2×2 km² GOCI I grid by bilinear interpolation. We use the GOCI I AOD for March 2011 through December 2020 and the GOCI II AOD for January 2021 through December 2022. We remove 1.7% of pixels in the GOCI II record with an AOD outside the range observed by GOCI I (-0.05 to 3.6). The GOCI II AOD retrieval is biased low over land relative to AERONET while GOCI I shows no significant bias (Lee et al., 2023). To avoid spurious trends in the inferred PM_{2.5}, we incorporate relevant training data into the RF as described in Section 2.4.

Bias-corrected GEOS-Chem monthly mean AOD. Following Pendergrass et al. (2022), we use bias-corrected GEOS-Chem CTM AODs to blend with GOCI I and II AODs in the gap-filling RF. The GEOS-Chem AODs are monthly means from a simulation by Zhai et al. (2021) for 2016 in East Asia with $0.5^\circ \times 0.625^\circ$ resolution. We bias-correct the GEOS-Chem AODs to match the annual mean GOCI



I and II AODs on the $2 \times 2 \text{ km}^2$ grid for each year in the 2011–2022 period. In this way, we obtain a spatial distribution of monthly mean bias-corrected GEOS-Chem AOD values.

Surface $\text{PM}_{2.5}$ data. We use hourly $\text{PM}_{2.5}$ data from operational air quality networks in eastern China, South Korea, and Japan, and average the data over 24 hours and over the $2 \times 2 \text{ km}^2$ GOCI AOD grid to define targets for the RF algorithm. Data for eastern China are from the National Environmental Monitoring Center (CNEMC; <https://quotsoft.net/air/>), with measurements in Beijing beginning in December 2013 and for the rest of the country in May 2014. Following Zhai et. al. (2019) we remove values with more than 24 consecutive repeats in the hourly timeseries as likely in error. Data in China are supplemented by US embassy data in Beijing (beginning in March 2011) and US consulates data in Shanghai (beginning in December 2011) and Shenyang (January 2013) (<https://www.airnow.gov/international/us-embassies-and-consulates>). These US embassy and consulates data have been used in previous air quality studies (Li et al., 2018; Pendergrass et al., 2019). Data for South Korea are from the AirKorea surface network (<https://www.airkorea.or.kr/>), which added $\text{PM}_{2.5}$ beginning in January 2015. Data for Japan are from the Japanese National Institute for Environmental Studies (NIES) for 2011–2021 (<https://tenbou.nies.go.jp/download/>) and for 2022 by the AEROS network (<https://soramame.env.go.jp/download>).

2.2 Gap-filled AOD and AOD missingness metric

The GOCI AOD records have gaps from clouds, snow cover, and other causes. Following Di et al. (2019), we perform gap-filling by using a separate GOCI AOD RF fit trained on the predictor variables of Table 1 except GOCI I and II AOD (the target variables in this case), the Gaspari-Cohn factor α (which has value 1 for all successful AOD retrievals), and the AirKorea surface air quality data. Because of the size of the AOD gap-filling problem, we use a separate RF for each year of data for computational economy. Training the GOCI AOD RF with annually disaggregated input data also avoids bias from gap-filling GOCI I based on information from GOCI II and vice versa. As shown in Figure 1, we find using a ten-fold crossvalidation that our GOCI AOD RF explains 91% of 24-h variability ($R^2 = 0.91$; annual $R^2 = 0.96$) with no significant mean bias. Our approach here improves on the statistical gap-filling method used in Pendergrass et al. (2022) which led to smooth AOD interpolation over large missing areas which may have been unphysical. To understand the variables driving the gap-filling prediction, we perform a SHAP analysis (lower panel) for a random sample of 0.1% of AOD data for 2016. NDVI is the most important predictor, perhaps because NDVI is predictive of AOD biases in both the GOCI I and II products (Choi et al., 2018; Lee et al., 2023), followed by GEOS-Chem modeled AOD and the six meteorological input variables; 2-m temperature and day of year are likely metrics for the seasonal variability of AOD.

The GOCI AOD gaps are non-random as they result from specific conditions that would not be part of the training dataset. However, Brokamp et al. (2018) found that when inferring $\text{PM}_{2.5}$ from AOD the non-randomness of AOD retrieval failure could be exploited to improve $\text{PM}_{2.5}$ predictions. Following Pendergrass et al. (2022), we compute an AOD missingness factor α that takes on a value of 1 if AOD is retrieved successfully at least once in a given day in a given grid cell and descending to 0 as distance to the nearest successful retrieval increases. We compute α with the Gaspari-Cohn function, a



polynomial with a single radial argument r that takes on a maximum value of 1 for $r = 0$ and a minimum value of 0 for $r \geq 2$ (Gaspari and Cohn, 1999). We obtain r for a given grid cell and day by normalizing the distance from the grid cell to that of the nearest AOD retrieval against an empirically determined spatial correlation length scale ranging from 110 km to 170 km across the domain (Pendergrass et al., 2022). By passing the Gaspari-Cohn factor α to the GOCI PM_{2.5} RF, we allow the algorithm to learn the optimal correction strategy in cases of AOD retrieval failure.

Evaluation of the GOCI AOD product for gap filling

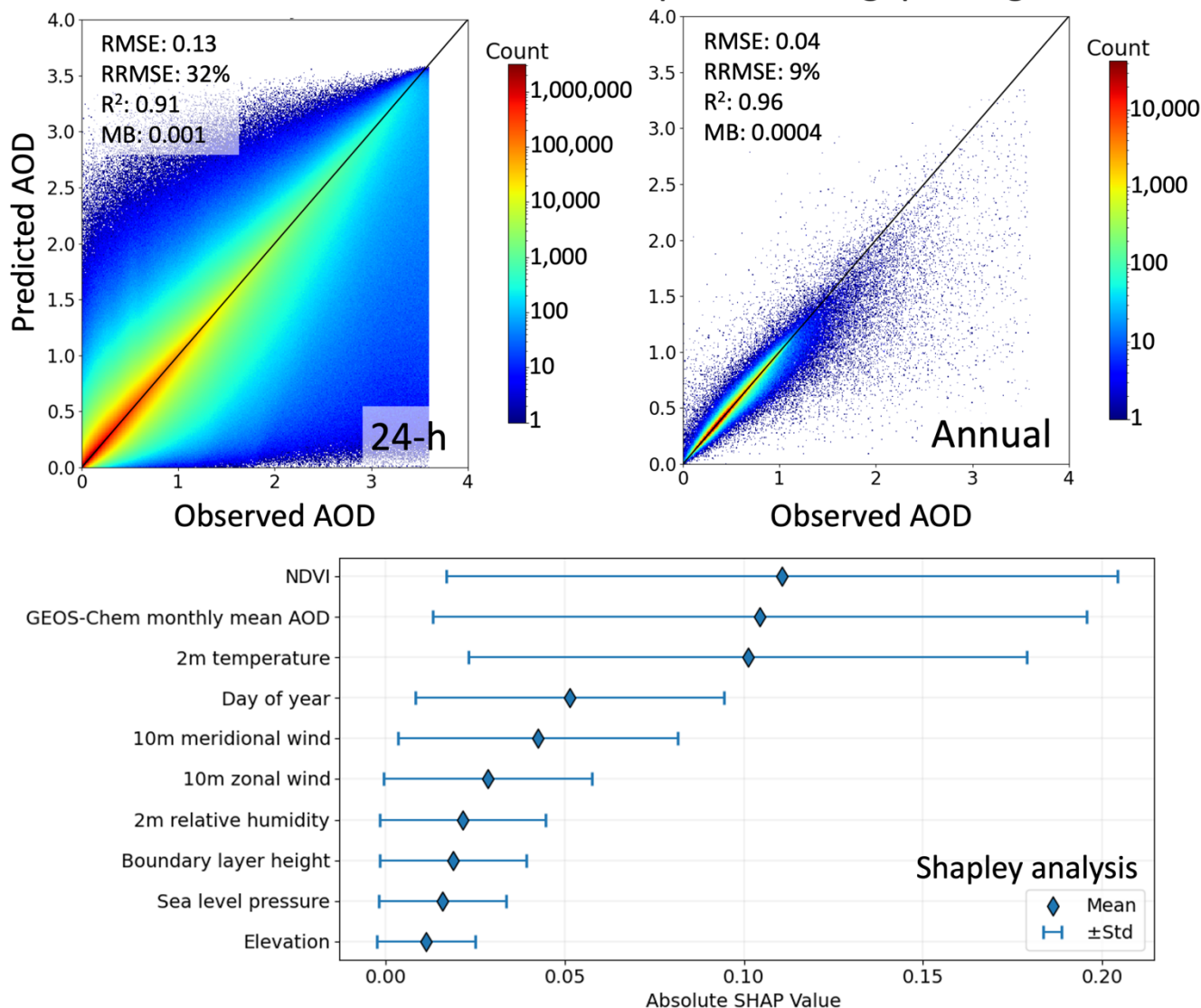


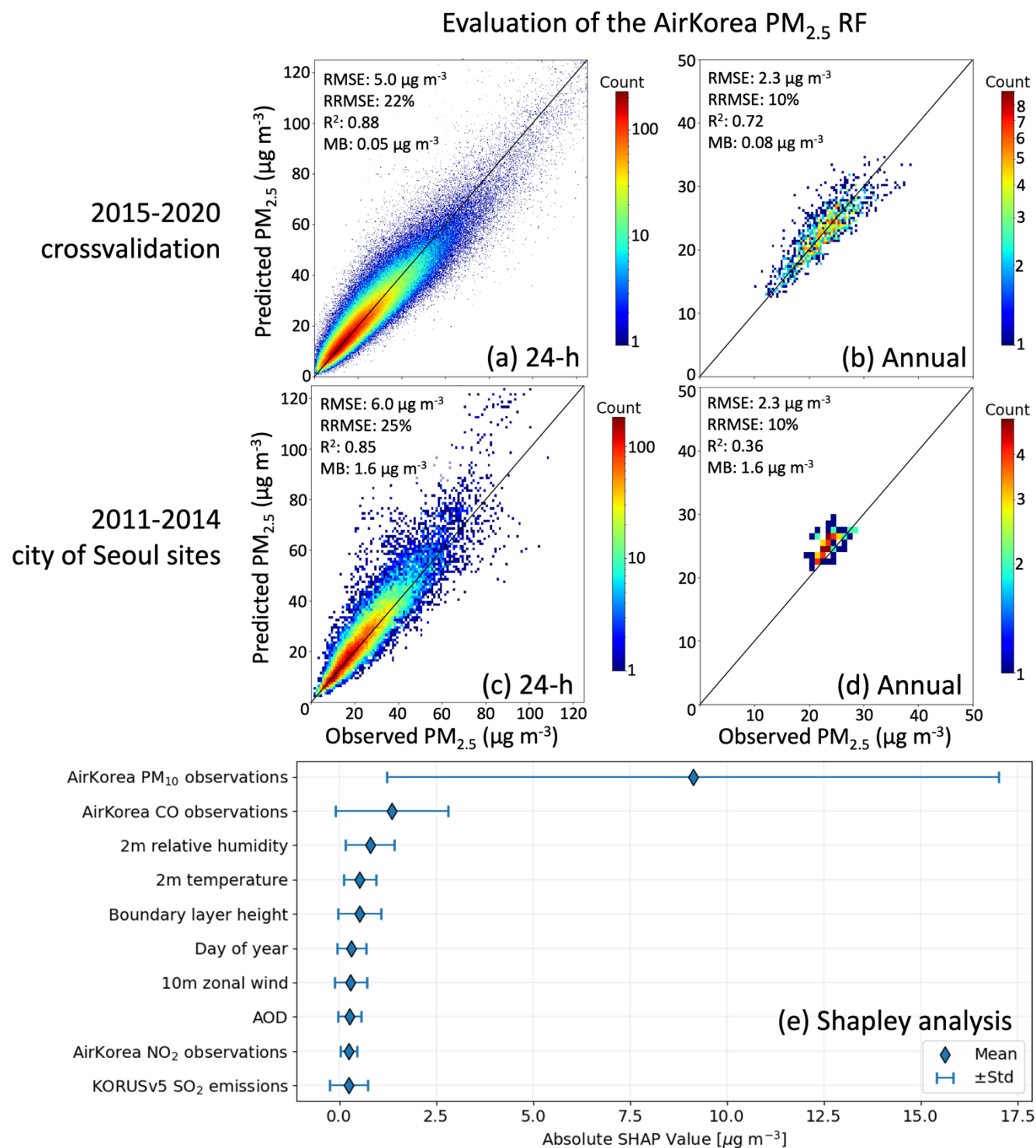
Figure 1: Evaluation of the GOCI AOD RF predictions. The top panels evaluate the GOCI AOD RF predictions in the 2011-22 training period at grid cells withheld entirely from training in a ten-fold crossvalidation procedure, aggregated at (a) 24-h and (b) annual resolution. Results are shown as two-dimensional histograms where pixel color corresponds to the count of observation/prediction correspondences within the corresponding bin, with statistics inset and the identity line shown in black. The bottom panel shows the top ten predictors of



AOD ranked by importance by the SHAP analysis. Predictor variable contributions are shown by mean absolute SHAP values and standard deviations.

225 2.3 Inferring South Korea PM_{2.5} before 2015

230 Prior to the January 2015 addition of PM_{2.5} measurements, the AirKorea surface network measured CO, O₃, NO₂, SO₂, and PM₁₀ concentrations. Many sites also recorded events of “yellow dust” transported from deserts in Mongolia and northern China (categorical true/false variable). We train a separate AirKorea PM_{2.5} RF on the 2015-2020 data, with all predictor variables in Table 1 except year and country categorical variables, to predict 24-h 2011-2014 PM_{2.5} at AirKorea sites. Figure 2 evaluates the ability of the AirKorea PM_{2.5} RF product by its ability to match observed PM_{2.5} in the 2015-2020 period. We find using a ten-fold crossvalidation that the AirKorea PM_{2.5} RF is able to predict 88% of 24-h PM_{2.5} variability in the 2015-2020 record with no significant bias.



235 Figure 2: Evaluation of the AirKorea PM_{2.5} RF predictions. The top panels evaluate the AirKorea PM_{2.5} RF predictions in the 2015-2020 training period at grid cells withheld entirely from training in a ten-fold crossvalidation procedure, aggregated at (a) 24-h and (b) annual resolution. Middle panels show an independent evaluation with observed 2011-2014 PM_{2.5} from the Seoul Research Institute surface network



in the city of Seoul, selecting the 20 sites that are collocated with AirKorea sites on the $2 \times 2 \text{ km}^2$ GOCI grid. Panels (a-d) show two-dimensional histograms where pixel color corresponds to the count of observation/prediction correspondences within the corresponding bin, with statistics inset and the identity line shown in black. The bottom panel shows the top ten predictors of AirKorea $\text{PM}_{2.5}$ ranked by importance by the SHAP analysis. Predictor variable contributions are shown by mean absolute SHAP values and standard deviations.

To independently evaluate the AirKorea $\text{PM}_{2.5}$ RF for the pre-2015 period, we use 2011-2014 hourly $\text{PM}_{2.5}$ data collected at 25 sites in the city of Seoul by the Seoul Research Institute of Public Health and Environment (NIER 2022) and select sites that are collocated with AirKorea sites within a $2 \times 2 \text{ km}^2$ GOCI grid cell (20 sites). We find that the AirKorea $\text{PM}_{2.5}$ RF reproduces successfully the 2011-2014 city of Seoul data (Figure 2), with statistics similar to the 2015-2020 crossvalidation. The annual R^2 is weak but this can be explained by the small sample size and small dynamic range. The most important predictor variable by far is PM_{10} , followed by CO and relative humidity. Figure 3 shows how the AirKorea $\text{PM}_{2.5}$ RF maps 2011-2014 PM_{10} data to infer $\text{PM}_{2.5}$.

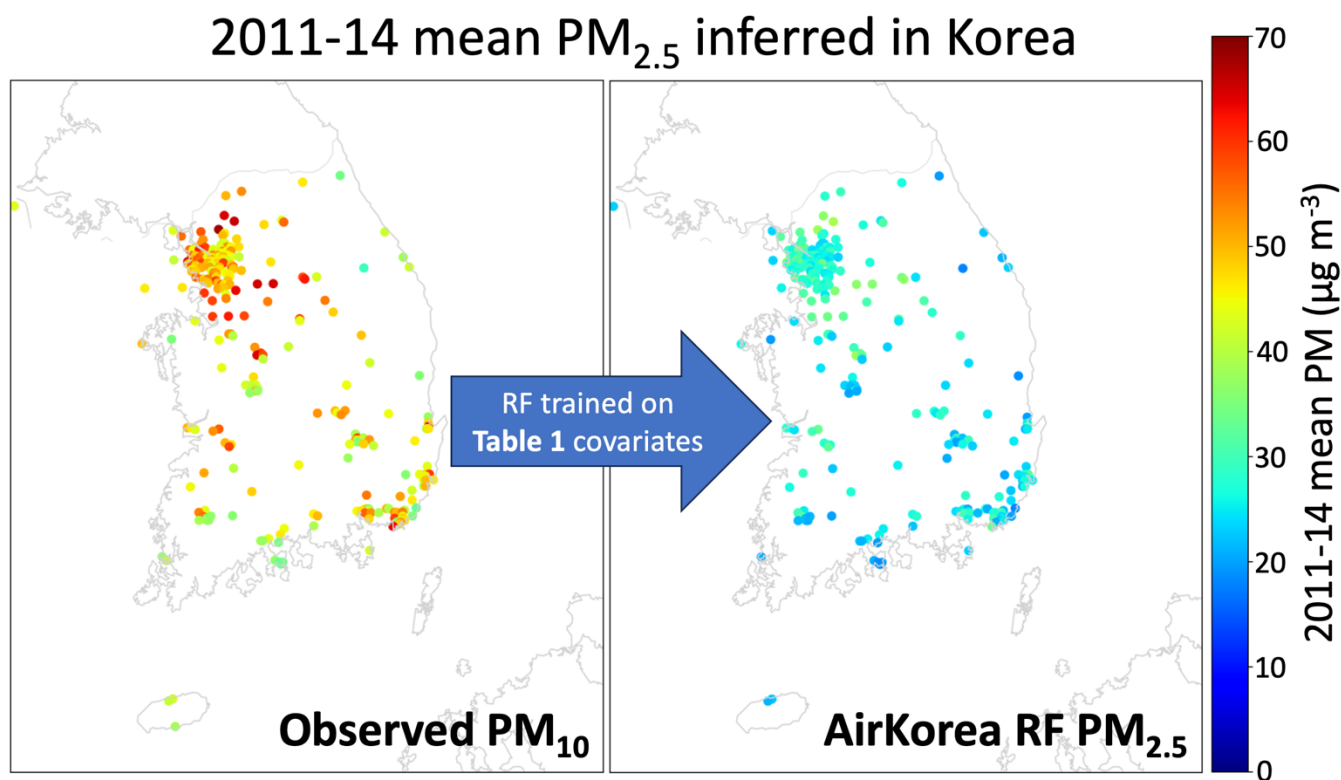


Figure 3: 2011-14 mean observed PM_{10} and inferred $\text{PM}_{2.5}$ at AirKorea sites. The AirKorea $\text{PM}_{2.5}$ RF is trained on data in Table 1 and its Shapley analysis is in Figure 2.

2.4 RF inference of $\text{PM}_{2.5}$ from GOCI AOD

After producing a gap-filled AOD dataset with the GOCI AOD RF and a 2011-2014 $\text{PM}_{2.5}$ target dataset for South Korea with the AirKorea $\text{PM}_{2.5}$ RF, we can infer continuous 24-h 2011-2022 $\text{PM}_{2.5}$ in the study domain at $2 \times 2 \text{ km}^2$ resolution. We train a GOCI $\text{PM}_{2.5}$ RF on all predictor variables in Table 1



for which we have gap-free coverage. The GOCI PM_{2.5} RF includes as its target all PM_{2.5} measurements
 260 from national networks, supplemented by PM_{2.5} from the US embassy and consulates in China and by
 the pre-2015 PM_{2.5} inferred in South Korea by the AirKorea PM_{2.5} RF.

We find that using year as a predictor variable substantially improves the GOCI PM_{2.5} RF fit, as
 its inclusion avoids an artificially large drop in PM_{2.5} concentrations from the 2020 to 2021-2022
 period, corresponding with the switch from the GOCI I instrument to GOCI II (section 2.1). However,
 265 in China prior to the 2014 start of surface network data, the use of year as a predictor is problematic
 because in that period PM_{2.5} is only available from the US embassy and consulates which is too sparse.
 To solve this problem, we train a separate China-rebalanced GOCI PM_{2.5} RF without year as a covariate
 and stopping in 2020 to avoid the GOCI II bias. In the China-rebalanced GOCI PM_{2.5} RF, we also apply
 training data weights to increase the penalty to the RF if the US embassy and consulate PM_{2.5} are poorly
 270 modeled prior to 2014. We use the output of the China-rebalanced GOCI PM_{2.5} RF to overwrite the
 GOCI PM_{2.5} RF output prior to May 2014 in China.

Figure 4 compares 24-h and annual mean PM_{2.5} network observations to predictions from the
 GOCI PM_{2.5} RF for sites in 2×2 km² grid cells withheld from training. Annual mean values are obtained
 by averaging the 24-h predictions. We find using a ten-fold crossvalidation that our prediction captures
 275 86% of the observed 24-h variance ($R^2 = 0.86$) and 95% of annual ($R^2 = 0.95$). Overall mean bias is
 only 0.26 µg m⁻³ but there are tail biases discussed later in this section. Applying the SHAP analysis to a
 random sample of 1% of the training data, we find that whether a grid cell is located in China is the
 most important predictor; this presumably serves as a proxy for the different vertical distribution of
 aerosols in the column relative to South Korea and Japan and also reflects the large dynamic range of
 280 PM_{2.5} in China. Boundary layer height and AOD are the most important physical predictors, as would
 be expected.

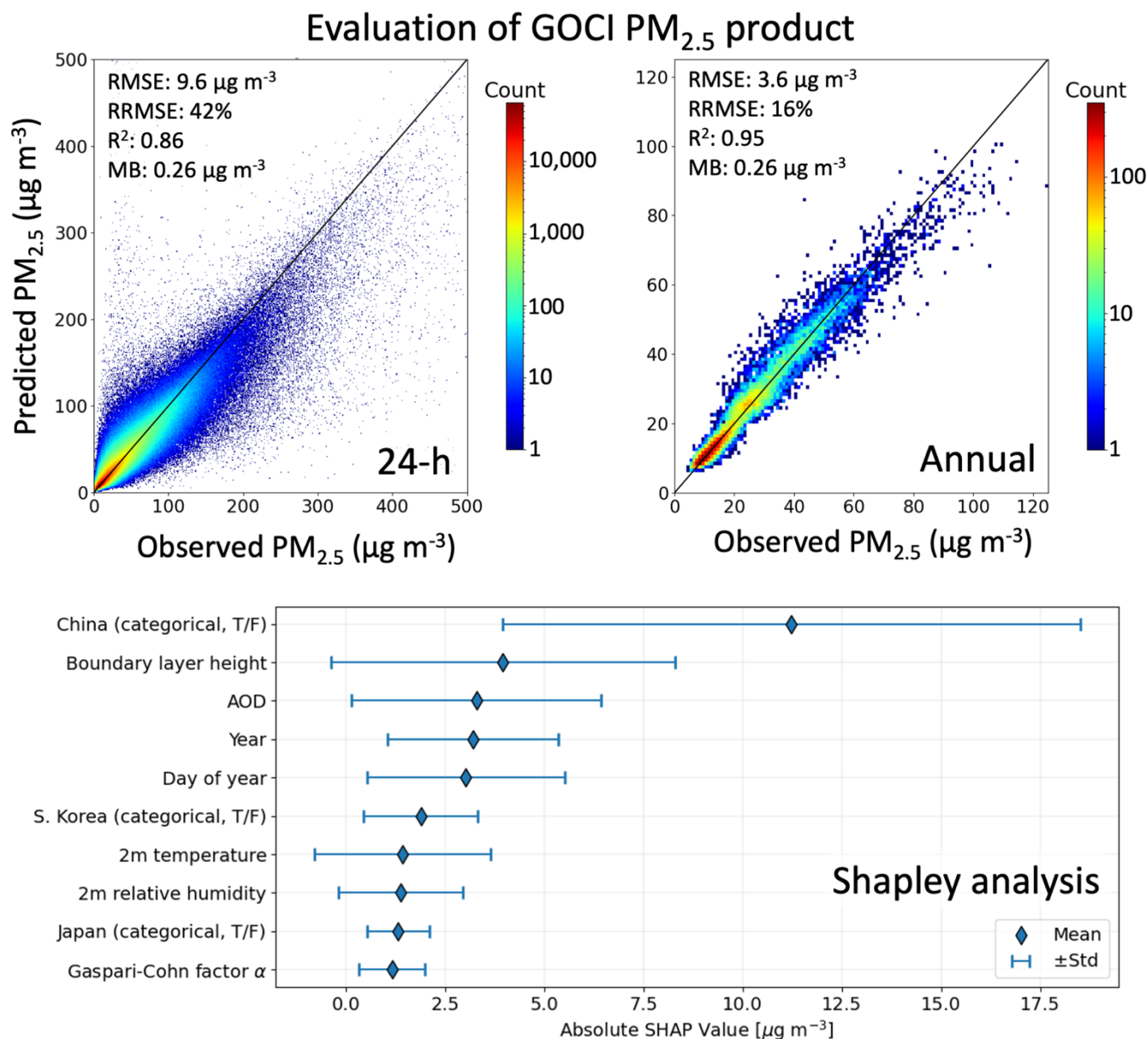


Figure 4: Evaluation of the GOCI PM_{2.5} RF predictions. The top panels evaluate the GOCI PM_{2.5} RF predictions in the 2011–2022 training period at grid cells withheld entirely from training in a ten-fold crossvalidation procedure, aggregated at (a) 24-h and (b) annual resolution. The panels show two-dimensional histograms where pixel color corresponds to the count of observation/prediction correspondences within the corresponding bin, with statistics inset and the identity line shown in black. The bottom panel shows the top ten predictors of GOCI PM_{2.5} ranked by importance by the SHAP analysis. Predictor variable contributions are shown by mean absolute SHAP values and standard deviations.

Figure 5 shows the performance of the GOCI PM_{2.5} product in the high tail of the distribution which is of particular interest for air pollution exposure but is notoriously difficult for RF algorithms to fit (Zhang and Lu, 2012; Pendergrass et al., 2022). Here, perhaps due to the very large training set, we



find that the RF extends the successful fit to the high tail. Averaging data into bins each containing 0.1% of ordered observations, we find that the observed 24-h 99th percentile of $129 \mu\text{g m}^{-3}$ is underestimated by 13.5% (annual by 7.6%) in the corresponding GOCI PM_{2.5} predictions. The observed 24-h 99.9th percentile of $319 \mu\text{g m}^{-3}$ is underestimated by GOCI PM_{2.5} by 26.5% (annual by 21.0%). These are relatively good RF performances for such high extremes.

GOCI PM_{2.5} prediction of the high tail of the PM_{2.5} distribution

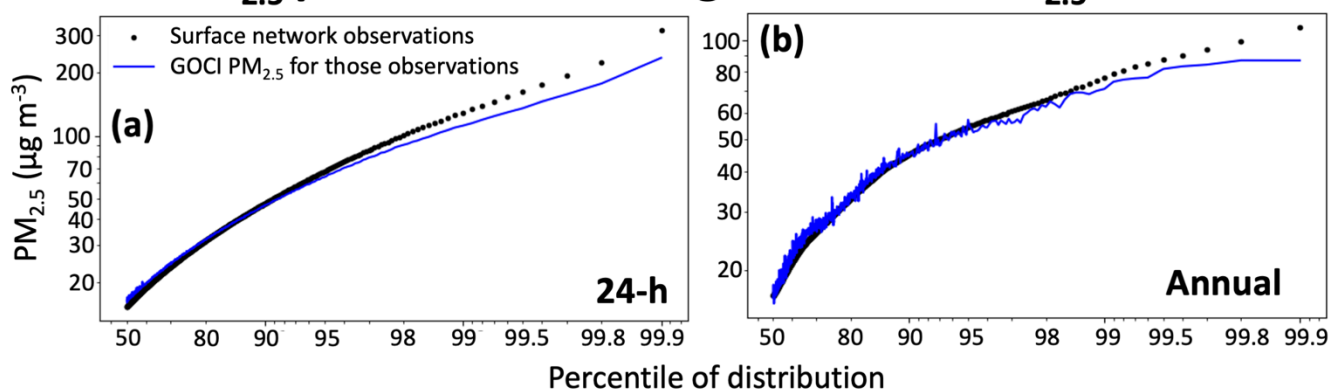


Figure 5: High tail of the PM_{2.5} distribution in China, South Korea, and Japan for 2011-2022. The figure shows the mean binned percentiles of the 24-h and annual PM_{2.5} concentrations measured at the surface networks, together with the corresponding mean GOCI PM_{2.5} predictions sampled at those observed percentiles.

3 Results and discussion

Here we present features and insights from our spatially and temporally continuous PM_{2.5} product generated from the GOCI AOD data from March 2011 to December 2022 with $2 \times 2 \text{ km}^2$ spatial resolution and 24-h temporal resolution. We refer to this product as GOCI PM_{2.5} in what follows. Results for annual data are presented starting in 2012 as the first full calendar year of data.

Figure 6 (top row) shows gap-filled GOCI AODs in 2012, 2017, and 2022. AOD declined steadily in East Asia over the lifetime of the GOCI I instrument (2011-2020) and drops sharply in the transition to GOCI II (2021-2022) but this is due partly to a low bias in GOCI II AOD. The middle row shows the PM_{2.5} network data, highlighting the spatial limitations as well as the temporal limitations before 2015. The bottom row shows our GOCI PM_{2.5} product, highlighting the spatial and temporal continuity over the period. The bias between GOCI I and II does not affect our GOCI PM_{2.5} product because the RF is given information to fit the GOCI data for individual years. The GOCI PM_{2.5} product shows high concentrations at the northeastern tip of China where there are no surface network data. Such high concentrations are not predicted in air quality models (Zhai et al., 2021) but have been previously inferred from MODIS AOD satellite observations (Van Donkelaar et al., 2021). They may be due to high ammonia emissions missing from current inventories (Kong et al., 2019), but also could be overestimated due to regional biases in vertical distributions of aerosols such as from Russian wildfires.

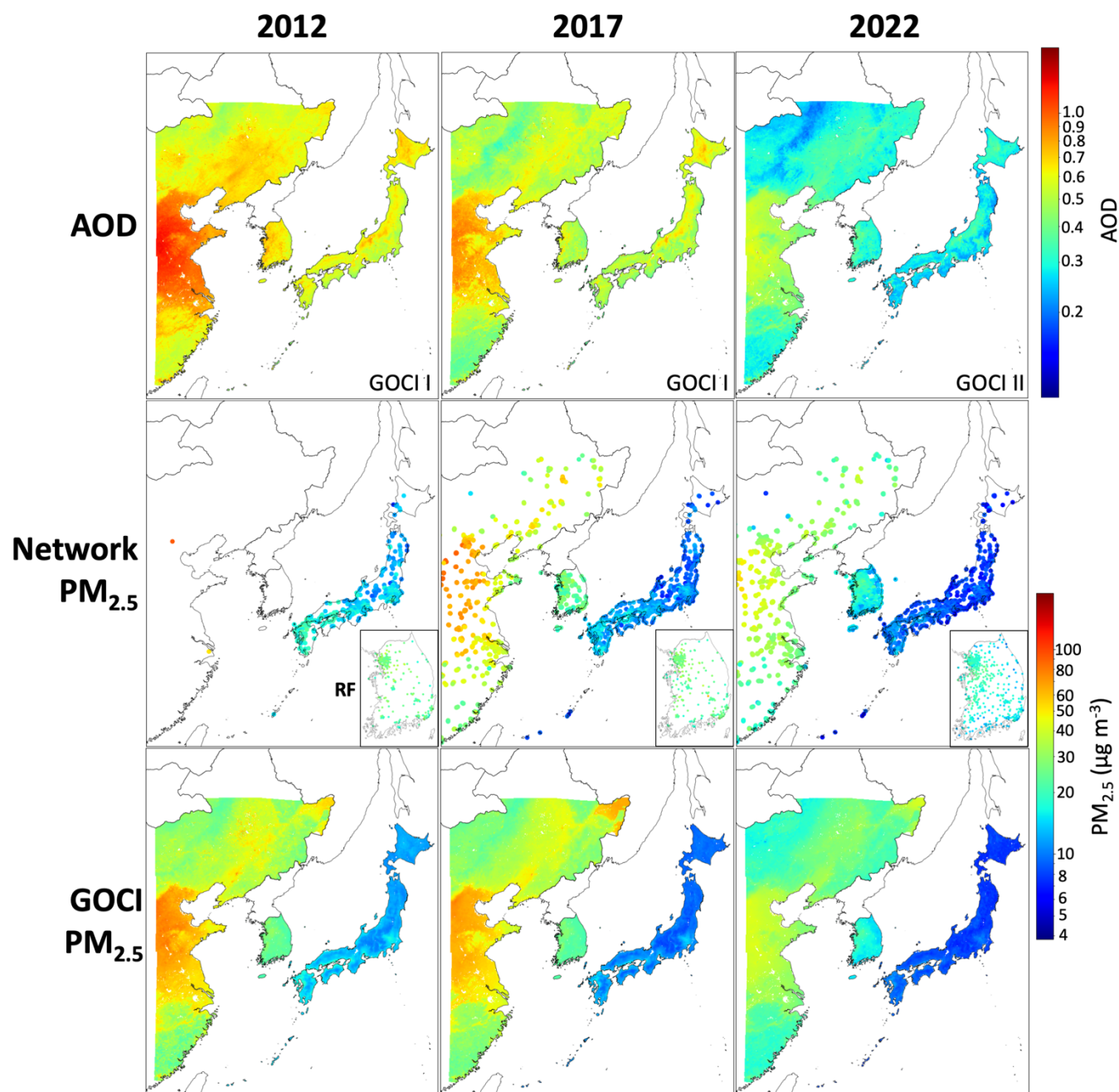


Figure 6: GOCI gap-filled aerosol optical depth (AOD), $PM_{2.5}$ from air quality networks, and GOCI $PM_{2.5}$ obtained by applying a RF algorithm to the GOCI AOD data. Data are annual means for 2012 (the first year with complete GOCI data), 2017, and 2022. The gap-filled AOD data provide continuous $2 \times 2 \text{ km}^2$ coverage of eastern China, S. Korea, and Japan for 2011–2022. The $PM_{2.5}$ network data are from individual sites and enlarged for visibility. The S. Korea insets in the middle panels provide greater resolution of network data gaps. $PM_{2.5}$ measurements from the AirKorea network started in 2015, and the S. Korea $PM_{2.5}$ network data shown for 2012 are from a RF reconstruction as described in Section 2.3.



Figure 7 shows long-term trends of annual GOCI $PM_{2.5}$ for each country with averaging weighted by area, population, and land type (Table 1). Also shown are the trends from the $PM_{2.5}$ networks, including pre-2015 data for Korea from our RF fit of other network data (Section 2.3). The GOCI $PM_{2.5}$ trends for the population-weighted average mirror the network trends and extrapolate them to before the start of the records. Peak concentrations were in 2014 (China) and 2013 (South Korea, Japan) and have been decreasing steadily since. The anomalous peak in South Korea $PM_{2.5}$ in 2019 is driven in part by unfavorable winter meteorological conditions (Cha et al., 2023). We find no COVID-19 anomaly in 2020, except perhaps in South Korea, possibly because emission decreases were offset by increase in oxidants producing secondary aerosol (Chang et al., 2020; Huang et al., 2021; Yang et al., 2022). We also see a narrowing spread with time across land use types and averaging method (areal or population-weighted), consistent with more rapid improvements in polluted urban areas.

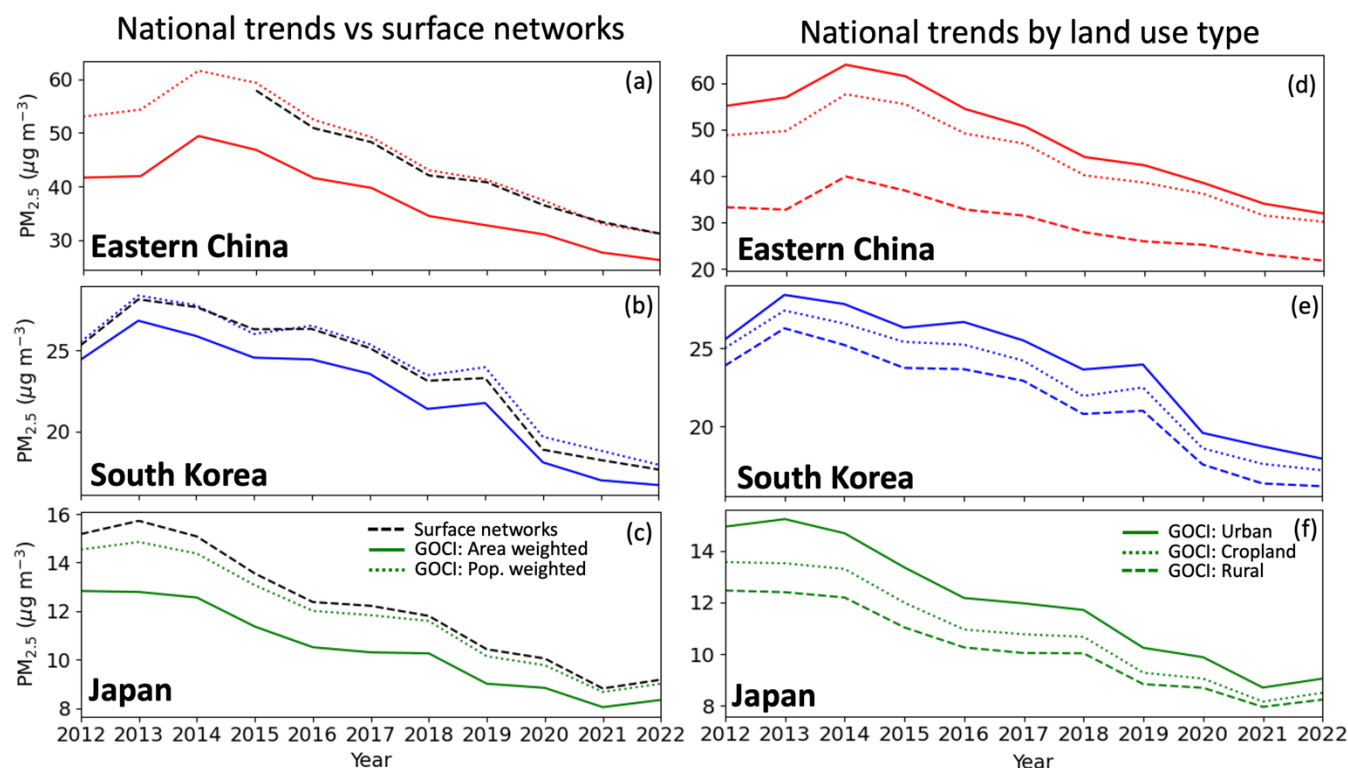


Figure 7: Trends in annual mean GOCI $PM_{2.5}$ concentrations averaged over eastern China, South Korea, and Japan for years with complete data (2012–2022). Also shown are the trends from the national $PM_{2.5}$ networks (dashed black lines) averaged over 2×2 km² grid cells and requiring at least 80% of data for a given year. Surface network data in South Korea prior to 2015 are generated from the AirKorea $PM_{2.5}$ RF using PM_{10} and other covariates (Table 1). GOCI $PM_{2.5}$ are shown as averages weighted by area, population, and land type.

Figure 8 compares our GOCI $PM_{2.5}$ product for Beijing to the US embassy observations going back to 2012, and places them in the context of $PM_{2.5}$ concentrations in the broader city. GOCI $PM_{2.5}$ tracks the observations at the US embassy well, peaking in 2013–2014 and then rapidly decreasing, a pattern consistent with the 2012–14 increase in $PM_{2.5}$ in East China shown in Figure 7. From the GOCI



350 $PM_{2.5}$ map we see that the US embassy was in a particularly polluted location in Beijing during the early part of the record but became more typical of the population-weighted city average after 2015. Improvements in $PM_{2.5}$ air quality in Beijing have been relatively greater than in other urban areas (Zhai et al., 2019), as is apparent from Figure 6.

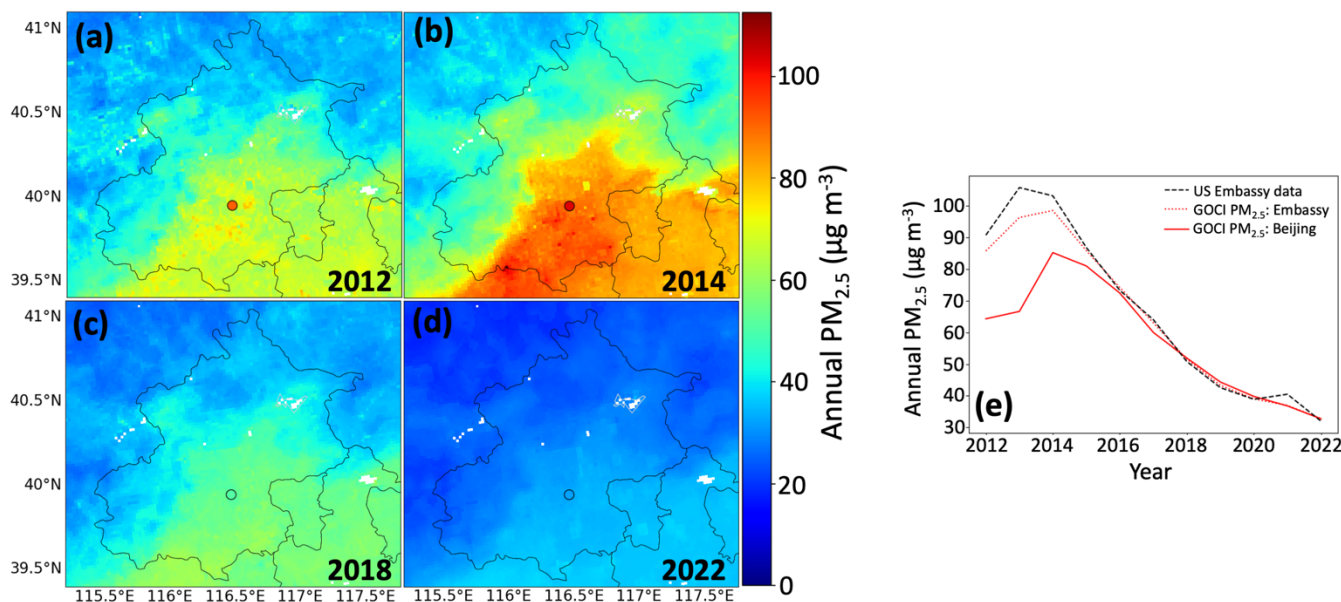
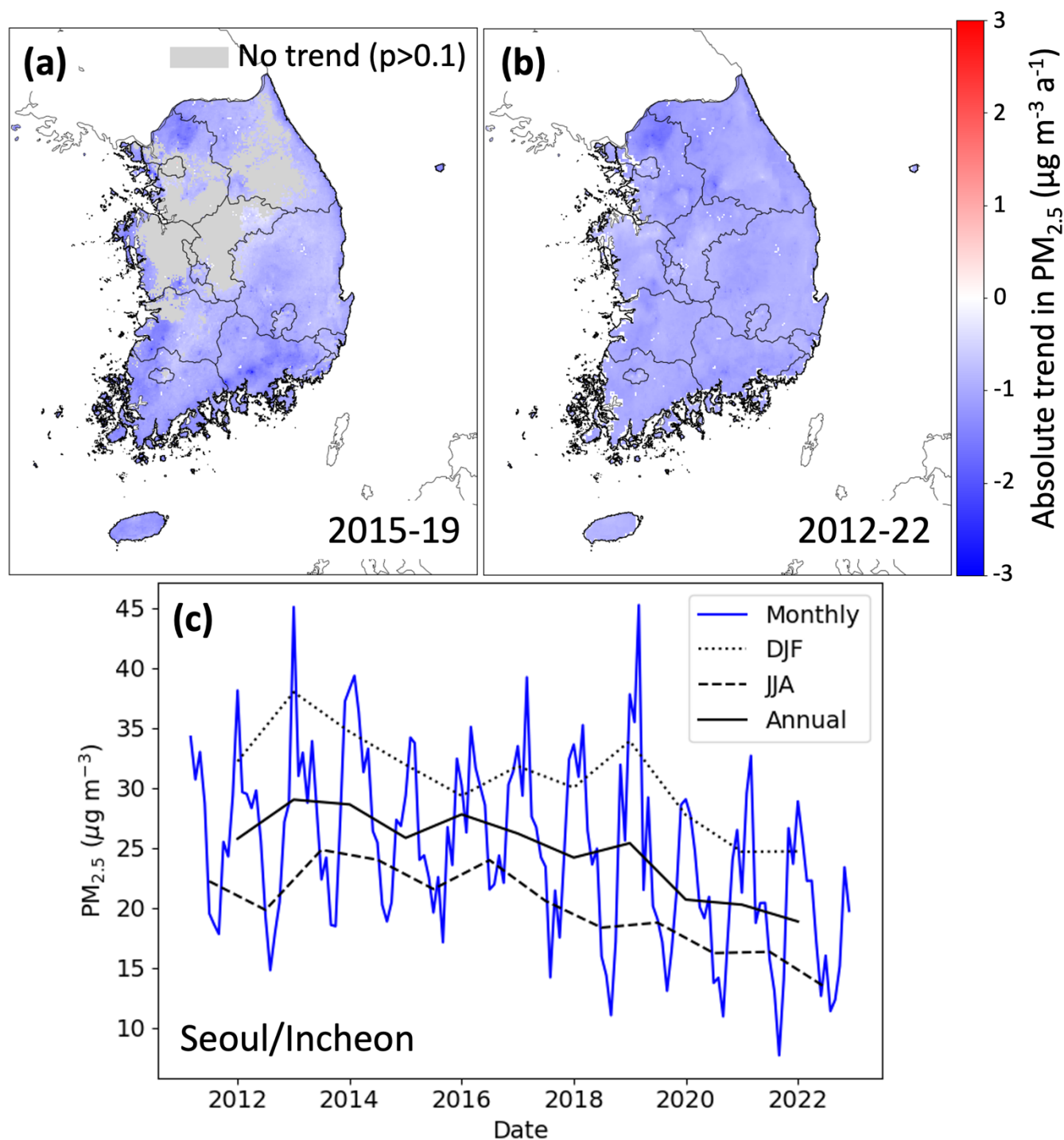


Figure 8: Annual mean GOCI $PM_{2.5}$ in Beijing compared with US embassy $PM_{2.5}$ observations in individual years. The left panels show the distribution of $PM_{2.5}$ in the city of Beijing (centered black outline) and surrounding area, with the location of the US embassy shown as a black circle. The right panel shows long-term trends at the US embassy site and averaged within Beijing city limits.

The long-term record produced in this work provides improved local information on 2011-2022 trends. Figure 9 shows trends in annual mean $PM_{2.5}$ concentrations in South Korea derived from a linear regression applied to the annual GOCI $PM_{2.5}$ in each 2×2 km² grid cell, as well as monthly trends in Seoul/Incheon starting in March 2011. The first five years of AirKorea $PM_{2.5}$ records (2015-19) showed no decrease in the Seoul metropolitan area (SMA) despite local emissions controls as well as controls upwind in China, and an increase in winter (Pendergrass et al., 2022). However, the 2012-2022 record shows steady improvements in $PM_{2.5}$ across the country including the SMA. The lack of trend in the 2015-2019 period in the SMA reflected the brevity of the record, as seen by the addition of the 2011-2015 years with the AirKorea $PM_{2.5}$ RF showing a decrease starting in 2013. Winter decrease after 2019 may have been further driven by a seasonal fine dust management program launched by the government of Seoul in 2019 that limits vehicle use, coal-fired power plants, and industrial activity from December through March (Ministry of the Environment, 2019; Yonhap News, 2021), but also may show an impact from COVID-19 lockdowns (Koo et al., 2020).



375 Figure 9: Trends in $PM_{2.5}$ concentrations in South Korea. Panels in the top row show annual trends for (a) 2015-2019 and (b) 2012-2022. The trends are obtained by ordinary linear regression of the annual mean GOCI $PM_{2.5}$ in each 2×2 km² grid cell with significant regression slope ($p < 0.10$). Grid cells with insignificant trends are plotted in gray. The bottom panel shows population-weighted GOCI $PM_{2.5}$



concentrations in Seoul and Incheon. Lines represent monthly (solid blue line), DJF (black dotted), JJA (black dashed), and annual (black solid) mean concentrations.

Figure 10 expresses the national trends in $PM_{2.5}$ in terms of population exposure. In China, where $PM_{2.5}$ air quality is worst, we find the greatest improvements for the populations exposed to the highest pollution, leading to a narrowing spread of exposures across the country that is illustrated by the sharpening slope of the cumulative distribution. While in 2014 97% of the population in China within the GOCI domain was exposed to annual $PM_{2.5}$ exceeding the national ambient air quality standard (NAAQS; $35 \mu g m^{-3}$), by 2022 the figure declined to 29%. However, over 99% of the population was still exposed to annual $PM_{2.5}$ greater than $15 \mu g m^{-3}$, the NAAQS in Japan and South Korea. In 2022 in South Korea 92% of the population still was exposed to annual $PM_{2.5}$ greater than the NAAQS but all would have met the pre-2018 NAAQS of $25 \mu g m^{-3}$. Japan was fully compliant with its NAAQS by 2018 and its air quality has continued to improve since, consistent with an observed shift from urban to marine aerosols over the study period (Kobayashi et al., 2023). Across the domain, the maximum to which any population is exposed decreases everywhere, which means that no population has been left behind in the improvements in $PM_{2.5}$ air quality.

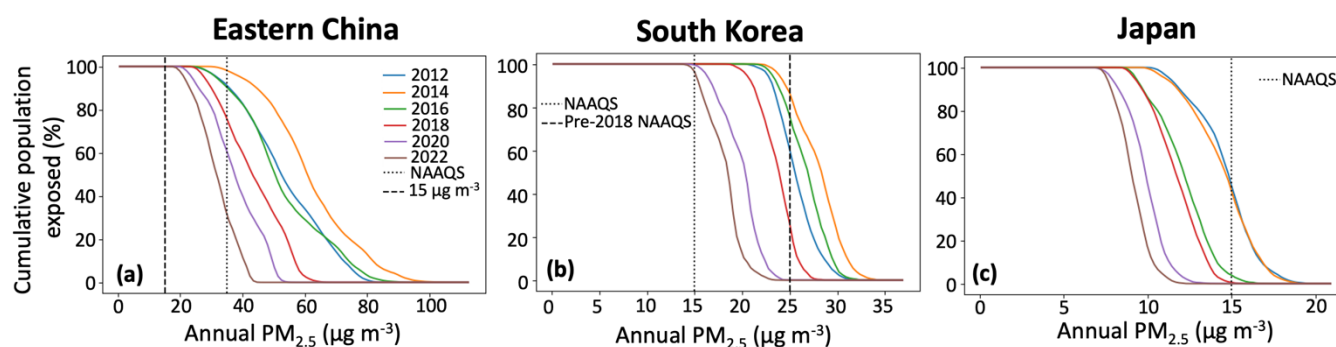


Figure 10: Trends in cumulative population exposure in countries within the study domain. The y axis shows the cumulative populations exposed to at least the annual $PM_{2.5}$ level given on the x axis, with year indicated by color. Panel (a) shows Eastern China, (b) South Korea, and (c) Japan. Note different scales for the different panels. National ambient air quality standards (NAAQS) are shown in the vertical black dotted line.

The $2 \times 2 km^2$ resolution of our new GOCI $PM_{2.5}$ product (compared to $6 \times 6 km^2$ in Pendergrass et al. (2022)) improves the representation of urban scale pollution events. This is illustrated in Figure 11 with a severe event in the SMA on 24–29 May 2016 previously shown by Pendergrass et al. (2022). Extreme concentrations and local gradients are better represented in the new product. Over the six-day period for the shown sites, we find an overall R^2 of 0.97 versus observations as compared with 0.77 for the $6 \times 6 km^2$ product in part because the resolution is now sharp enough to individually resolve all sites. A two-sample Kolmogorov-Smirnov test indicates that the $6 \times 6 km^2$ product has a statistically significantly different distribution than the observations ($p < 0.001$) while the improved $2 \times 2 km^2$ product is indistinguishable ($p = 0.52$).

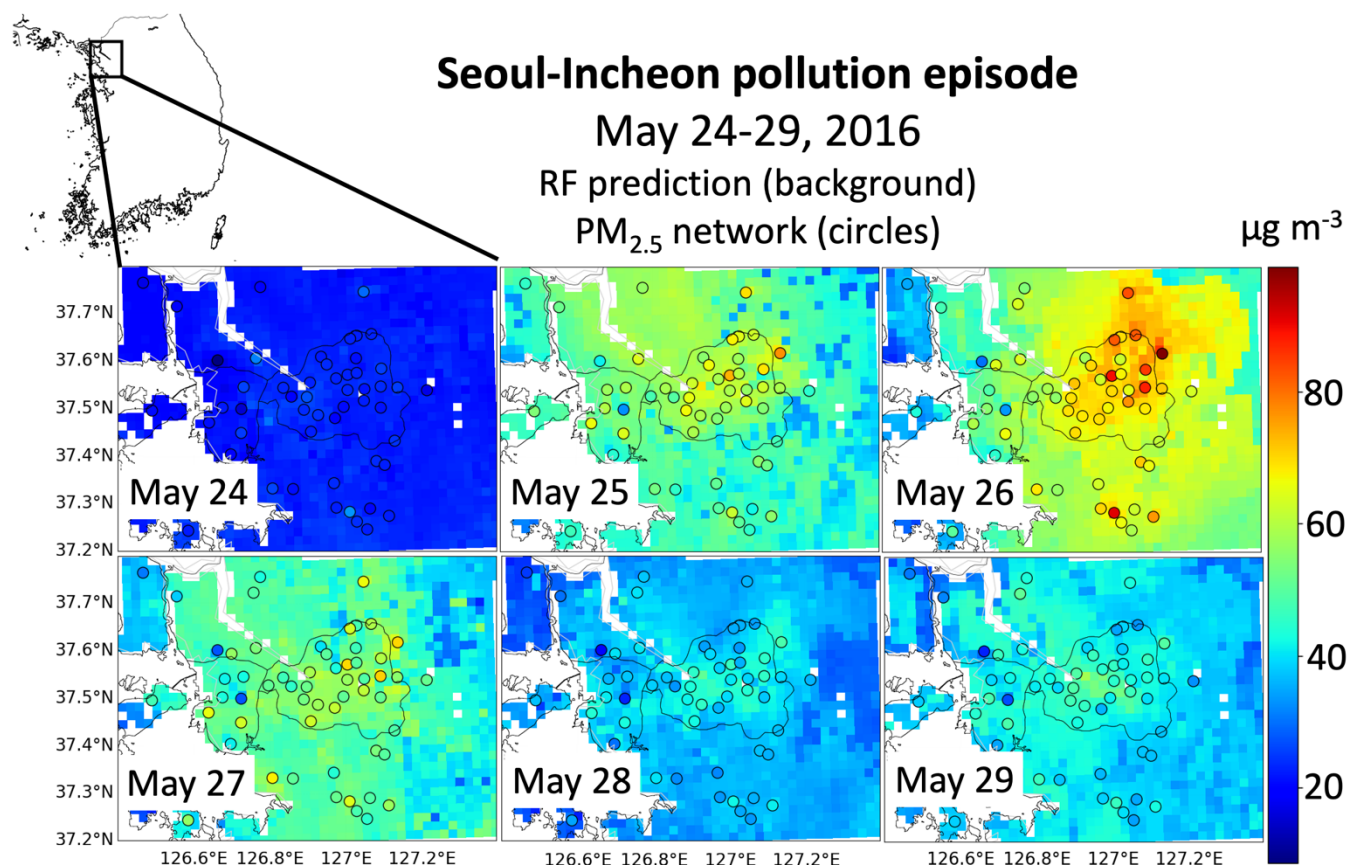


Figure 11: 24 h PM_{2.5} concentrations during a pollution event in the Seoul Metropolitan Area (24–29 May 2016). Observations from the AirKorea surface network (circles) are overlaid on GOCI PM_{2.5} produced in this work (2×2 km² grid). Seoul city limits are shown by the black outline in the panel center.

4 Conclusions

We produced a continuous 24-h data set of fine particulate matter (PM_{2.5}) concentrations over East Asia at 2×2 km² resolution for 2011–2022 by training a random forest (RF) machine learning algorithm on GOCI I and II geostationary satellite observations of aerosol optical depth (AOD) to predict PM_{2.5} observations from surface networks. The resulting GOCI PM_{2.5} dataset offers high-resolution coverage of the region over a twelve-year period of rapid change. It improves on our previous GOCI PM_{2.5} product (Pendergrass et al., 2022) in spatial resolution, record duration, and RF method.

We produced the GOCI PM_{2.5} data in a three-step process. First, we gap-filled missing GOCI I and II AOD retrievals using an RF algorithm trained on covariates including gap size, chemical transport model (CTM) output, meteorology, and land use variables. Second, to train on the GOCI I data starting in March 2011, before the start of PM_{2.5} monitoring in South Korea (2015), we trained another RF to predict 2011–2014 PM_{2.5} at AirKorea network sites using the pre-2015 data available at those sites and most notably PM₁₀. Finally, we used the gap-filled GOCI AOD along with the target



PM_{2.5} set expanded by the inferred 2011-2014 AirKorea PM_{2.5} and US embassy and consulate data in pre-2014 China to train an RF to predict PM_{2.5} across the study domain.

The continuous 2011-2022 GOCI PM_{2.5} record at 2×2 km² resolution constructed in this manner reproduces the PM_{2.5} network observations with no significant bias and a relative root-mean-square error (RRMSE) of 22% for 24-h data and 10% for annual data. Its success extends to the high tail of the PM_{2.5} frequency distribution (severe pollution episodes). It shows that the air quality networks in all three countries are representative of population-weighted exposure. The 2012-2022 full-year time series show PM_{2.5} peaking in 2014 (China) and 2013 (South Korea and Japan) and then steadily declining through the end of 2022 with steepest improvements in the most polluted regions. Population exposure over that period decreases for all quantiles of the distributions, implying that no region has been left behind in air quality improvement. While the Seoul Metropolitan Area (SMA) does not show a decrease over the first five years of the PM_{2.5} network record (2015-2019), the longer 2012-2022 record shows a decline consistent with the rest of the country.

The 2×2 km² resolution of our GOCI PM_{2.5} product enables successful representation of the fine-scale structure and statistical distribution of concentrations during urban pollution episodes, improving significantly on our previous 6×6 km² product that had excessive smoothing. It should be of value for long-term public health studies where continuity of PM_{2.5} data is essential.

Data availability 24-h 2×2 km² resolution 24-h GOCI PM_{2.5} from March 1, 2011 through December 31, 2022 are made publicly available on DataVerse (<https://doi.org/10.7910/DVN/0GO7BS>, Pendergrass et al., 2024). PM_{2.5} data for eastern China are publicly available from the National Environmental Monitoring Center (<https://quotsoft.net/air/>); data for South Korea are available from AirKorea (<https://www.airkorea.or.kr/>); data for Japan for 2011-2021 are available from the National Institute for Environmental Studies (NIES) (<https://tenbou.nies.go.jp/download/>) and for 2022 from the AEROS network (<https://soramame.env.go.jp/download>). The versions of GOCI I and GOCI II AOD data used in this paper are available on request to the corresponding author. All other input data to the RF is publicly available at links given in the text and can also be provided on request.

Author Contributions DP and DJJ designed the study. DP developed the RF and performed analysis. SZ ran and analyzed chemical transport model data. SL and JL aided in satellite data processing. MK, HI, and YO aided in surface data processing. JK, DJJ, and HL provided scientific interpretation and discussion. All authors provided input on the paper for revision before submission.

Competing interests The authors declare that they have no conflict of interest.

Acknowledgements This work was funded by the Samsung PM_{2.5} Strategic Research Program and the Harvard-NUIST Joint Laboratory for Air Quality and Climate (JLAQC). GOCI data was provided by the Korea Institute of Marine Science & Technology Promotion (KIMST) funded by the Ministry of Oceans and Fisheries (20220546). DCP was funded in part by a US National Science Foundation Graduate Fellowship.



References

- 465 Alduchov, O. A., & Eskridge, R. E. (1996). Improved Magnus Form Approximation of Saturation Vapor Pressure. *Journal of Applied Meteorology*, 35(4), 601–609. [https://doi.org/10.1175/1520-0450\(1996\)035<0601:IMFAOS>2.0.CO;2](https://doi.org/10.1175/1520-0450(1996)035<0601:IMFAOS>2.0.CO;2)
- Bae, M., Kim, B.-U., Kim, H. C., Kim, J., and Kim, S.: Role of emissions and meteorology in the recent PM_{2.5} changes in China and South Korea from 2015 to 2018, *Environmental Pollution*, 270, 116233, <https://doi.org/10.1016/j.envpol.2020.116233>, 2021.
- 470 Brasseur, G. P. and Jacob, D. J: *Modeling of Atmospheric Chemistry*, Cambridge University Press, Cambridge, U.K., 2017.
- Breiman, L.: Random Forests, *Mach. Learn.*, 45, 5–32, <https://doi.org/10.1023/A:1010933404324>, 2001.
- Brokamp, C., Jandarov, R., Hossain, M., and Ryan, P.: Predicting Daily Urban Fine Particulate Matter Concentrations Using a Random Forest Model, *Environ. Sci. Technol.*, 52, 4173–4179, <https://doi.org/10.1021/acs.est.7b05381>, 2018.
- 475 Burnett, R., Chen, H., Szyszkowicz, M., Fann, N., Hubbell, B., Pope, C. A., Apte, J. S., Brauer, M., Cohen, A., Weichenthal, S., Coggins, J., Di, Q., Brunekreef, B., Frostad, J., Lim, S. S., Kan, H., Walker, K. D., Thurston, G. D., Hayes, R. B., ... Spadaro, J. V. (2018). Global estimates of mortality associated with long-term exposure to outdoor fine particulate matter. *Proceedings of the National Academy of Sciences*, 115(38), 9592–9597. <https://doi.org/10.1073/pnas.1803222115>
- 480 Center for International Earth Science Information Network CIESIN – Columbia University: Gridded Population of the World, Version 4 (GPWv4): Population Density, Revision 11, NASA Socioeconomic Data and Applications Center (SEDAC) [dataset], <https://doi.org/10.7927/H49C6VHW>, 2018.
- 485 Chang, Y., Huang, R.-J., Ge, X., Huang, X., Hu, J., Duan, Y., Zou, Z., Liu, X., & Lehmann, M. F. (2020). Puzzling Haze Events in China During the Coronavirus (COVID-19) Shutdown. *Geophysical Research Letters*, 47(12), e2020GL088533. <https://doi.org/10.1029/2020GL088533>
- 490 Cha Y, Song C-K, Jeon K, et al. (2023) Factors affecting recent PM_{2.5} concentrations in China and South Korea from 2016 to 2020. *Science of The Total Environment* 881: 163524.
- Chinese State Council (2013). Action Plan on Air Pollution Prevention and Control, available at: http://www.gov.cn/zwggk/2013-09/12/content_2486773.htm (last access: 1 September 2023).
- 495 Cho, Y., Kim, J., Go, S., Kim, M., Lee, S., Kim, M., Chong, H., Lee, W.-J., Lee, D.-W., Torres, O., & Park, S. S. (2023a). First Atmospheric Aerosol Monitoring Results from Geostationary Environment Monitoring Spectrometer (GEMS) over Asia. *Atmospheric Measurement Techniques Discussions*, 1–29. <https://doi.org/10.5194/amt-2023-221>
- Cho, Y., Kim, J., Lee, J., Choi, M., Lim, H., Lee, S., & Im, J. (2023b). Fine particulate concentrations over East Asia derived from aerosols measured by the advanced Himawari Imager using machine learning. *Atmospheric Research*, 290, 106787. <https://doi.org/10.1016/j.atmosres.2023.106787>
- 500 Choi, J.-K., Park, Y. J., Ahn, J. H., Lim, H.-S., Eom, J., & Ryu, J.-H. (2012). GOCI, the world's first geostationary ocean color observation satellite, for the monitoring of temporal variability in



- coastal water turbidity. *Journal of Geophysical Research: Oceans*, 117(C9).
 505 <https://doi.org/10.1029/2012JC008046>
- Choi, M., Kim, J., Lee, J., Kim, M., Park, Y.-J., Jeong, U., Kim, W., Hong, H., Holben, B., Eck, T. F.,
 Song, C. H., Lim, J.-H., & Song, C.-K. (2016). GOCI Yonsei Aerosol Retrieval (YAER)
 algorithm and validation during the DRAGON-NE Asia 2012 campaign. *Atmospheric
 Measurement Techniques*, 9(3), 1377–1398. <https://doi.org/10.5194/amt-9-1377-2016>
- 510 Choi, M., Kim, J., Lee, J., Kim, M., Park, Y.-J., Holben, B., Eck, T. F., Li, Z., & Song, C. H. (2018).
 GOCI Yonsei aerosol retrieval version 2 products: An improved algorithm and error analysis
 with uncertainty estimation from 5-year validation over East Asia. *Atmospheric Measurement
 Techniques*, 11(1), 385–408. <https://doi.org/10.5194/amt-11-385-2018>
- Choi, W., Ho, C.-H., Heo, J.-W., Kim, K.-Y., Kim, S.-W., & Kim, J. (2022). Recent Air Quality
 515 Deterioration on Weekends in Seoul, South Korea: A Focus on External Contribution. *Asia-
 Pacific Journal of Atmospheric Sciences*. <https://doi.org/10.1007/s13143-022-00287-0>
- Copernicus Climate Change Service, Climate Data Store (CDS), (2019): Land cover classification
 gridded maps from 1992 to present derived from satellite observation. Copernicus Climate
 Change Service (C3S) Climate Data Store (CDS). DOI: [10.24381/cds.006f2c9a](https://doi.org/10.24381/cds.006f2c9a)
- 520 Danielson, J.J., and Gesch, D.B., 2011, *Global multi-resolution terrain elevation data 2010
 (GMTED2010)*: U.S. Geological Survey Open-File Report 2011-1073,
<http://pubs.usgs.gov/of/2011/1073/pdf/of2011-1073.pdf>.
- van Donkelaar, A., Hammer, M. S., Bindle, L., Brauer, M., Brook, J. R., Garay, M. J., Hsu, N. C.,
 Kalashnikova, O. V., Kahn, R. A., Lee, C., Levy, R. C., Lyapustin, A., Sayer, A. M., & Martin,
 525 R. V. (2021). Monthly Global Estimates of Fine Particulate Matter and Their Uncertainty.
Environmental Science & Technology, 55(22), 15287–15300.
<https://doi.org/10.1021/acs.est.1c05309>
- Di, Q., Amini, H., Shi, L., Kloog, I., Silvern, R., Kelly, J., Sabath, M. B., Choirat, C., Koutrakis, P.,
 Lyapustin, A., Wang, Y., Mickley, L. J., & Schwartz, J. (2019). An ensemble-based model of
 530 PM_{2.5} concentration across the contiguous United States with high spatiotemporal resolution.
Environment International, 130, 104909. <https://doi.org/10.1016/j.envint.2019.104909>
- Dominici, F., Peng, R. D., Bell, M. L., Pham, L., McDermott, A., Zeger, S. L., & Samet, J. M. (2006).
 Fine particulate air pollution and hospital admission for cardiovascular and respiratory diseases.
JAMA, 295(10), 1127–1134. <https://doi.org/10.1001/jama.295.10.1127>
- 535 Gaspari, G., & Cohn, S. E. (1999). Construction of correlation functions in two and three dimensions.
Quarterly Journal of the Royal Meteorological Society, 125(554), 723–757.
<https://doi.org/10.1002/qj.49712555417>
- Guo, B., Zhang, D., Pei, L., Su, Y., Wang, X., Bian, Y., Zhang, D., Yao, W., Zhou, Z., & Guo, L.
 (2021). Estimating PM_{2.5} concentrations via random forest method using satellite, auxiliary,
 540 and ground-level station dataset at multiple temporal scales across China in 2017. *Science of The
 Total Environment*, 778, 146288. <https://doi.org/10.1016/j.scitotenv.2021.146288>
- Huang, X., Ding, A., Gao, J., Zheng, B., Zhou, D., Qi, X., Tang, R., Wang, J., Ren, C., Nie, W., Chi, X.,
 Xu, Z., Chen, L., Li, Y., Che, F., Pang, N., Wang, H., Tong, D., Qin, W., ... He, K. (2021).
 Enhanced secondary pollution offset reduction of primary emissions during COVID-19



- lockdown in China. *National Science Review*, 8(2), nwaa137.
<https://doi.org/10.1093/nsr/nwaa137>
- Ito, A., Wakamatsu, S., Morikawa, T., & Kobayashi, S. (2021). 30 Years of Air Quality Trends in Japan. *Atmosphere*, 12(8), Article 8. <https://doi.org/10.3390/atmos12081072>
- Jeong, J. I., Park, R. J., Song, C.-K., Yeh, S.-W., & Woo, J.-H. (2024). Quantitative analysis of winter PM_{2.5} reduction in South Korea, 2019/20 to 2021/22: Contributions of meteorology and emissions. *Science of The Total Environment*, 907, 168179.
<https://doi.org/10.1016/j.scitotenv.2023.168179>
- Jo, Y.-J., Lee, H.-J., Jo, H.-Y., Woo, J.-H., Kim, Y., Lee, T., Heo, G., Park, S.-M., Jung, D., Park, J., & Kim, C.-H. (2020). Changes in inorganic aerosol compositions over the Yellow Sea area from impact of Chinese emissions mitigation. *Atmospheric Research*, 240, 104948.
<https://doi.org/10.1016/j.atmosres.2020.104948>
- Joo, H.-S. Comprehensive Plan on Fine Dust Management. Korea Environmental Policy Bulletin, 15(2), No. 46. <https://me.go.kr/home/file/readDownloadFile.do?fileId=148570&fileSeq=6>, 2018.
- Kim, M., Kim, J., Lim, H., Lee, S., Cho, Y., Lee, Y.-G., Go, S., & Lee, K. (2023). AOD data fusion with Geostationary Korea Multi-Purpose Satellite (Geo-KOMPSAT) instruments GEMS, AMI, and GOCI-II: Statistical and deep neural network methods. *Atmospheric Measurement Techniques Discussions*, 1–34. <https://doi.org/10.5194/amt-2023-255>
- Kioumourtzoglou Marianthi-Anna, Schwartz Joel D., Weisskopf Marc G., Melly Steven J., Wang Yun, Dominici Francesca, & Zanobetti Antonella. (2016). Long-term PM_{2.5} Exposure and Neurological Hospital Admissions in the Northeastern United States. *Environmental Health Perspectives*, 124(1), 23–29. <https://doi.org/10.1289/ehp.1408973>
- Kobayashi, H., Irie, H., Momoi, M., Ohno, T., Yamamoto, H., Khatri, P., Sano, I., Okumura, H., & Kobayashi, H. (2023). Development and Classification of Japanese-Region-Specific Aerosol Models Based on 10-Year Sky Radiometer Observations. *Sola*, 19, 210–216.
<https://doi.org/10.2151/sola.2023-027>
- Koo, J.-H., Kim, J., Lee, Y. G., Park, S. S., Lee, S., Chong, H., Cho, Y., Kim, J., Choi, K., & Lee, T. (2020). The implication of the air quality pattern in South Korea after the COVID-19 outbreak. *Scientific Reports*, 10(1), 22462. <https://doi.org/10.1038/s41598-020-80429-4>
- Kong, L., Tang, X., Zhu, J., Wang, Z., Pan, Y., Wu, H., Wu, L., Wu, Q., He, Y., Tian, S., Xie, Y., Liu, Z., Sui, W., Han, L., & Carmichael, G. (2019). Improved Inversion of Monthly Ammonia Emissions in China Based on the Chinese Ammonia Monitoring Network and Ensemble Kalman Filter. *Environmental Science & Technology*, 53(21), 12529–12538.
<https://doi.org/10.1021/acs.est.9b02701>
- Kulkarni, P., Sreekanth, V., Upadhy, A. R., & Gautam, H. C. (2022). Which model to choose? Performance comparison of statistical and machine learning models in predicting PM_{2.5} from high-resolution satellite aerosol optical depth. *Atmospheric Environment*, 282, 119164.
<https://doi.org/10.1016/j.atmosenv.2022.119164>
- Muñoz-Sabater, J., Dutra, E., Agustí-Panareda, A., Albergel, C., Arduini, G., Balsamo, G., Boussetta, S., Choulga, M., Harrigan, S., Hersbach, H., Martens, B., Miralles, D. G., Piles, M., Rodríguez-Fernández, N. J., Zsoter, E., Buontempo, C., & Thépaut, J.-N. (2021). ERA5-Land: A state-of-



- the-art global reanalysis dataset for land applications. *Earth System Science Data*, 13(9), 4349–4383. <https://doi.org/10.5194/essd-13-4349-2021>
- National Institute of Environmental Research (NIER). Annual report of air quality in Korea 2022. Available from: https://www.airkorea.or.kr/web/detailViewDown?pMENU_NO=125 (in Korean). Last accessed: 13 March 2024.
- 590 Lee, S., Choi, M., Kim, J., Kim, M. and Lim, H. (2017). Retrieval of aerosol optical depth with high spatial resolution using GOCI data. *Korean Journal of Remote Sensing*, 33(6-1), 961-970.
- Lee, S., Choi, M., Kim, J., Park, Y.-J., Choi, J.-K., Lim, H., Lee, J., Kim, M., & Cho, Y. (2023). Retrieval of aerosol optical properties from GOCI-II observations: Continuation of long-term
 595 geostationary aerosol monitoring over East Asia. *Science of The Total Environment*, 903, 166504. <https://doi.org/10.1016/j.scitotenv.2023.166504>
- Li, K., Liao, H., Cai, W., & Yang, Y. (2018). Attribution of Anthropogenic Influence on Atmospheric Patterns Conducive to Recent Most Severe Haze Over Eastern China. *Geophysical Research Letters*, 45(4), 2072–2081. <https://doi.org/10.1002/2017GL076570>
- 600 Li, W., Xu, L., Liu, X., Zhang, J., Lin, Y., Yao, X., Gao, H., Zhang, D., Chen, J., Wang, W., Harrison, R. M., Zhang, X., Shao, L., Fu, P., Nenes, A., & Shi, Z. (2017). Air pollution–aerosol interactions produce more bioavailable iron for ocean ecosystems. *Science Advances*, 3(3), e1601749. <https://doi.org/10.1126/sciadv.1601749>
- Li, Y., Dai, Z., & Liu, X. (2018). Analysis of Spatial-Temporal Characteristics of the PM_{2.5}
 605 Concentrations in Weifang City, China. *Sustainability*, 10(9), Article 9. <https://doi.org/10.3390/su10092960>
- Lim H, Choi M, Kim J, et al. (2018) AHI/Himawari-8 Yonsei Aerosol Retrieval (YAER): Algorithm, Validation and Merged Products. *Remote Sensing* 10(5). 5. Multidisciplinary Digital Publishing Institute: 699.
- 610 Liu, Y., Li, C., Liu, D., Tang, Y., Seyler, B. C., Zhou, Z., Hu, X., Yang, F., & Zhan, Y. (2022). Deriving hourly full-coverage PM_{2.5} concentrations across China’s Sichuan Basin by fusing multisource satellite retrievals: A machine-learning approach. *Atmospheric Environment*, 271, 118930. <https://doi.org/10.1016/j.atmosenv.2021.118930>
- 615 Park, S., Shin, M., Im, J., Song, C.-K., Choi, M., Kim, J., Lee, S., Park, R., Kim, J., Lee, D.-W., & Kim, S.-K. (2019). Estimation of ground-level particulate matter concentrations through the synergistic use of satellite observations and process-based models over South Korea. *Atmospheric Chemistry and Physics*, 19(2), 1097–1113. <https://doi.org/10.5194/acp-19-1097-2019>
- Pedregosa, F., Varoquaux, G., Gramfort, A., Michel, V., Thirion, B., Grisel, O., Blondel, M., Prettenhofer, P., Weiss, R., Dubourg, V., Vanderplas, J., Passos, A., Cournapeau, D., Brucher, M., Perrot, M., & Duchesnay, É. (2011). Scikit-learn: Machine Learning in Python. *Journal of Machine Learning Research*, 12(85), 2825–2830.
- 620 Pendergrass, D. C., Shen, L., Jacob, D. J., & Mickley, L. J. (2019). Predicting the Impact of Climate Change on Severe Wintertime Particulate Pollution Events in Beijing Using Extreme Value Theory. *Geophysical Research Letters*, 46(3), 1824–1830. <https://doi.org/10.1029/2018GL080102>
- 625



- Pendergrass, D. C., Zhai, S., Kim, J., Koo, J.-H., Lee, S., Bae, M., Kim, S., Liao, H., & Jacob, D. J. (2022). Continuous mapping of fine particulate matter (PM_{2.5}) air quality in East Asia at daily 6  ×  6 km² resolution by application of a random forest algorithm to 2011–2019 GOCI geostationary satellite data. *Atmospheric Measurement Techniques*, 15(4), 1075–1091. <https://doi.org/10.5194/amt-15-1075-2022>
- Pendergrass, D. C., Jacob, D. J., Oak, Y. J., Lee, J., Kim, M., Kim, J., Lee, S., Zhai, S., Irie, H., & Liao, H. (2024). Continuous 2011–2022 record of fine particulate matter (PM_{2.5}) in East Asia at daily 2-km resolution from GOCI I and II satellite observations [dataset]. Harvard Dataverse. <https://doi.org/10.7910/DVN/0G07BS>
- She, Q., Choi, M., Belle, J. H., Xiao, Q., Bi, J., Huang, K., Meng, X., Geng, G., Kim, J., He, K., Liu, M., & Liu, Y. (2020). Satellite-based estimation of hourly PM_{2.5} levels during heavy winter pollution episodes in the Yangtze River Delta, China. *Chemosphere*, 239, 124678. <https://doi.org/10.1016/j.chemosphere.2019.124678>
- Song, C., Liu, B., Cheng, K., Cole, M. A., Dai, Q., Elliott, R. J. R., & Shi, Z. (2023). Attribution of Air Quality Benefits to Clean Winter Heating Policies in China: Combining Machine Learning with Causal Inference. *Environmental Science & Technology*, 57(46), 17707–17717. <https://doi.org/10.1021/acs.est.2c06800>
- Szopa, S., V. Naik, B. Adhikary, P. Artaxo, T. Bernsten, W.D. Collins, S. Fuzzi, L. Gallardo, A. Kiendler-Scharr, Z. Klimont, H. Liao, N. Unger, and P. Zanis, 2021: Short-Lived Climate Forcers. In *Climate Change 2021: The Physical Science Basis. Contribution of Working Group I to the Sixth Assessment Report of the Intergovernmental Panel on Climate Change* [Masson-Delmotte, V., P. Zhai, A. Pirani, S.L. Connors, C. Péan, S. Berger, N. Caud, Y. Chen, L. Goldfarb, M.I. Gomis, M. Huang, K. Leitzell, E. Lonnoy, J.B.R. Matthews, T.K. Maycock, T. Waterfield, O. Yelekçi, R. Yu, and B. Zhou (eds.)]. Cambridge University Press, Cambridge, United Kingdom and New York, NY, USA, pp. 817–922, doi: 10.1017/9781009157896.008.
- Tan, Y., Wang, Q., & Zhang, Z. (2023). Coupling the linear mixed effects model with random forest improves hourly PM_{2.5} estimation from Himawari-8 AOD over the Yangtze River Delta. *Atmospheric Pollution Research*, 14(5), 101739. <https://doi.org/10.1016/j.apr.2023.101739>
- Tang, Y., Deng, R., Liang, Y., Zhang, R., Cao, B., Liu, Y., Hua, Z., & Yu, J. (2023). Estimating high-spatial-resolution daily PM_{2.5} mass concentration from satellite top-of-atmosphere reflectance based on an improved random forest model. *Atmospheric Environment*, 302, 119724. <https://doi.org/10.1016/j.atmosenv.2023.119724>
- Tie, X., Huang, R.-J., Dai, W., Cao, J., Long, X., Su, X., Zhao, S., Wang, Q., & Li, G. (2016). Effect of heavy haze and aerosol pollution on rice and wheat productions in China. *Scientific Reports*, 6(1), Article 1. <https://doi.org/10.1038/srep29612>
- Vermote, Eric; NOAA CDR Program. (2019): NOAA Climate Data Record (CDR) of AVHRR Normalized Difference Vegetation Index (NDVI), Version 5. NOAA National Centers for Environmental Information. <https://doi.org/10.7289/V5ZG6QH9>.
- Wang, Y., Duan, X., & Wang, L. (2019). Spatial-Temporal Evolution of PM_{2.5} Concentration and its Socioeconomic Influence Factors in Chinese Cities in 2014–2017. *International Journal of Environmental Research and Public Health*, 16(6), Article 6. <https://doi.org/10.3390/ijerph16060985>



- Wei, Y., Wang, Y., Di, Q., Choirat, C., Wang, Y., Koutrakis, P., Zanobetti, A., Dominici, F., &
 Schwartz, J. D. (2019). Short term exposure to fine particulate matter and hospital admission
 risks and costs in the Medicare population: Time stratified, case crossover study. *BMJ*, 367,
 16258. <https://doi.org/10.1136/bmj.16258>
- Wongnaka, P., Chitchum, P., Sripramong, R., & Phosri, A. (2023). Application of satellite remote
 sensing data and random forest approach to estimate ground-level PM_{2.5} concentration in
 Northern region of Thailand. *Environmental Science and Pollution Research*, 30(38), 88905–
 88917. <https://doi.org/10.1007/s11356-023-28698-0>
- Woo, J.-H., Kim, Y., Kim, H.-K., Choi, K.-C., Eum, J.-H., Lee, J.-B., Lim, J.-H., Kim, J., & Seong, M.
 (2020). Development of the CREATE Inventory in Support of Integrated Climate and Air
 Quality Modeling for Asia. *Sustainability*, 12(19), Article 19.
<https://doi.org/10.3390/su12197930>
- Xie, P., & Liao, H. (2022). The Impacts of Changes in Anthropogenic Emissions Over China on PM_{2.5}
 Concentrations in South Korea and Japan During 2013–2017. *Frontiers in Environmental
 Science*, 10. <https://www.frontiersin.org/article/10.3389/fenvs.2022.841285>
- Xu, J.-W., Martin, R. V., van Donkelaar, A., Kim, J., Choi, M., Zhang, Q., Geng, G., Liu, Y., Ma, Z.,
 Huang, L., Wang, Y., Chen, H., Che, H., Lin, P., & Lin, N. (2015). Estimating ground-level
 PM_{2.5} in eastern China using aerosol optical depth determined from the GOCI satellite
 instrument. *Atmospheric Chemistry and Physics*, 15(22), 13133–13144.
<https://doi.org/10.5194/acp-15-13133-2015>
- Yang, J., Wang, S., Zhang, R., & Yin, S. (2022). Elevated particle acidity enhanced the sulfate
 formation during the COVID-19 pandemic in Zhengzhou, China. *Environmental Pollution*, 296,
 118716. <https://doi.org/10.1016/j.envpol.2021.118716>
- Zhai, S., Jacob, D. J., Wang, X., Shen, L., Li, K., Zhang, Y., Gui, K., Zhao, T., & Liao, H. (2019). Fine
 particulate matter (PM_{2.5}) trends in China, 2013–2018: Separating contributions from
 anthropogenic emissions and meteorology. *Atmospheric Chemistry and Physics*, 19(16), 11031–
 11041. <https://doi.org/10.5194/acp-19-11031-2019>
- Zhai, S., Jacob, D. J., Brewer, J. F., Li, K., Moch, J. M., Kim, J., Lee, S., Lim, H., Lee, H. C., Kuk, S.
 K., Park, R. J., Jeong, J. I., Wang, X., Liu, P., Luo, G., Yu, F., Meng, J., Martin, R. V., Travis,
 K. R., ... Liao, H. (2021). Relating geostationary satellite measurements of aerosol optical depth
 (AOD) over East Asia to fine particulate matter (PM_{2.5}): Insights from the KORUS-AQ aircraft
 campaign and GEOS-Chem model simulations. *Atmospheric Chemistry and Physics*, 21(22),
 16775–16791. <https://doi.org/10.5194/acp-21-16775-2021>
- Zhai, S., Jacob, D. J., Wang, X., Liu, Z., Wen, T., Shah, V., Li, K., Moch, J. M., Bates, K. H., Song, S.,
 Shen, L., Zhang, Y., Luo, G., Yu, F., Sun, Y., Wang, L., Qi, M., Tao, J., Gui, K., ... Liao, H.
 (2021). Control of particulate nitrate air pollution in China. *Nature Geoscience*, 1–7.
<https://doi.org/10.1038/s41561-021-00726-z>
- Zhao, D., Chen, H., Sun, X., & Shi, Z. (2018). Spatio-temporal Variation of PM_{2.5} Pollution and its
 Relationship with Meteorology among Five Megacities in China. *Aerosol and Air Quality
 Research*, 18(9), 2318–2331. <https://doi.org/10.4209/aaqr.2017.09.0351>
- Zhang, J., Liu, L., Xu, L., Lin, Q., Zhao, H., Wang, Z., Guo, S., Hu, M., Liu, D., Shi, Z., Huang, D., &
 Li, W. (2020). Exploring wintertime regional haze in northeast China: Role of coal and biomass



burning. Atmospheric Chemistry and Physics, 20(9), 5355–5372. <https://doi.org/10.5194/acp-20-5355-2020>

Zou, Eric Yongchen. “Unwatched Pollution: The Effect of Intermittent Monitoring on Air Quality.” American Economic Review 111, no. 7 (July 2021): 2101–26.
<https://doi.org/10.1257/aer.20181346>.

715